Subsonic and Transonic Aerodynamics of a Wraparound Fin Configuration

G. L. Winchenbach* and Randy S. Buff†
Air Force Armament Laboratory, Eglin Air Force Base, Florida
and
Robert H. Whyte‡ and Wayne H. Hathaway‡
General Electric Company, Burlington, Vermont

Subsonic and transonic aerodynamic data for a wraparound fin configuration are presented. Free-flight aeroballistic tests to obtain these data were conducted at atmospheric pressure and over a Mach number range of 0.6 to 1.35. The aerodynamic coefficients and derivatives presented were extracted from the position-attitude-time histories of the experimentally measured trajectories using nonlinear numerical integration data reduction routines. Results of this analysis indicate that a dynamic instability exists above Mach 1.0 and is related to an out-of-plane side moment which is dependent on the pitch angle. The stability boundaries associated with this side moment are mapped. Designers should consider this moment whenever wraparound fins are used.

Nomenclature

A = reference area, $\Pi d^2/4$
a_c = Coriolis acceleration
AF = amplification factor
C_ℓ = roll amount coefficient $\ell/\bar{q}Ad$
$C_{\ell p}$ = slope of the roll moment vs spin
$C_{\ell_{\gamma\alpha}}$ = induced roll moment derivative
C_m = pitching moment coefficient $m/\bar{q}Ad$
C_{mq} = pitch damping derivative $(\partial C_m)/[\partial(qd)/(2V)]$
C_{mq2} = quadratic pitch damping coefficient
C_{m_α} = slope of pitching moment vs α
$C_{m\alpha3}, C_{m\alpha5}$ = cubic and fifth order pitching moment coefficients
$C_{m_{\alpha_M}}$ = slope of pitching moment derivative vs Mach number
C_N = normal force coefficient $F_N/\bar{q}A$
C_{N_α} = slope of the normal force vs α
$C_{N\alpha3}, C_{N\alpha5}$ = cubic and fifth order normal force coefficient
C_n = side moment coefficient $n/\bar{q}Ad$
C_{n_α} = slope of side moment vs α
C_{np_α} = Magnus moment derivative
C_X = axial force coefficient (axial force)/$(\bar{q}A)$
C_{X_0} = axial force coefficient at zero angle of attack
C_{X_M} = slope of axial force coefficient vs Mach number
d = body diameter and reference length
g = acceleration due to gravity
I_x, I_y = moments of inertia about the x and y axis
K_{10}, K_{20} = magnitude of linear theory vectors
K_T = magnitude of trim vector
L = model length
ℓ, m, n = roll, pitch, and yaw moments, respectively
$\hat{m}$ = model mass
M = Mach number
p, q, r = rolling, pitching, and yawing velocities, respectively
$\bar{q}$ = dynamic pressure
R_{e_L} = Reynolds number based on model length
u, v, w = velocities in the X, Y, and Z direction, respectively
X, Y, Z = fixed plane coordinates
V = total velocity
α = total angle of attack
α_M = maximum total angle of attack
γ = aerodynamic roll angle
θ, ψ, ϕ = rotation angles
ω_{10}, ω_{20} = linear theory vector frequencies
λ_1, λ_2 = linear theory vector damping rates
$\bar{\delta}^2$ = effective angle of attack squared

Superscripts

$(\dot{})$ = first derivative with respect to time
$(\bar{})$ = total values

Introduction

BECAUSE of packaging advantages, designers of tube-launched and dispenser-launched submunitions have used wraparound fin (WAF) designs for years.[1-3] These designs permit the fins to be neatly folded around the body prior to launch. This saves valuable space and allows either the maximum number or size of submunitions to be packaged in the dispenser or tube. Upon launch the fins are deployed to provide the required aerodynamic stability during flight. However, many of these past designs have experienced unusual and adverse flight dynamics.[4] Many of these problems were thought to be related to the erratic rolling motion of the munition caused by the WAF design.[5-6] During a recent test program it was observed that some of the models displayed unusual damping characteristics (generally unfavorable). The analysis of the experimentally measured motion profiles indicated that these unfavorable damping characteristics were caused by the existence of an out-of-plane (side) moment due to pitch angle.

The purpose of this paper is to describe these recent free-flight aerodynamic tests, present the data obtained, and discuss the ramifications of the out-of-plane moment. The stability boundaries of this side moment are developed and indicate that this configuration is dynamically stable subsonically and unstable supersonically. It is suspected that this side

Presented as Paper 85-0106 at the AIAA 23rd Aerospace Sciences Meeting, Reno, NV, Jan. 14-17, 1985; received Feb. 1, 1985; revision received March 20, 1986.

*Chief, Aeroballistics Section, Aeromechanics Division. Senior Member AIAA.
†Project Engineer, Aeromechanics Division. Member AIAA.
‡Advanced Munitions Engineer. Member AIAA.

moment is symptomatic of WAF configurations and should be of particular concern to the designer.

Facilities, Models, and Test Conditions

Free Flight Range

The free flight tests were conducted at the Air Force Armament Laboratory, Eglin Air Force Base, Florida. The test facility[7] is an enclosed, atmospheric, instrumented, concrete structure used to examine the exterior ballistics of various free-flight configurations. The facility contains a gun room, control room, model measurement room, blast chamber, and the instrumented range.

The 207-m instrumented length of the range has a 3.66-m^2 cross section for the first 69 m and a 4.88-m^2 cross section for the remaining length. The range has 131 locations available as instrumentation sites. Each location has a physical separation of 1.52 m: presently 50 of the sites are used to house fully instrumented orthogonal shadowgraph stations. The maximum shadowgraph window, an imaginary circle in which a projectile in flight will cast a shadow on both reflective screens, is 2.13 m in diameter. The nominal operating temperature of the range is 22° C.

Models and Test Conditions

The overall model geometry and WAF details are shown in the sketches of Fig. 1. Fourteen of these models were flown in the facility during the test program, 11 flights were successfully analyzed, and aerodynamic coefficients and derivatives extracted. The tests were conducted at atmospheric pressure and over a Mach number range of 0.58 to 1.35. The measured physical properties of each of the models and the associated test conditions for each of the eleven flights successfully analyzed are presented in Table 1.

The models were launched from a 152 mm, inside diameter, smooth bore compressed gas launcher using a conventional four-piece sabot. No attempt was made to augment the initial angular disturbances of the models as the model/sabot package exited the launcher.

Free-Flight Data Reduction

Extraction of the aerodynamic coefficients and derivatives is the primary goal in analyzing the trajectories measured in free flight. This is accomplished by using the Aeroballistic Research Facility Data Analysis System (ARFDAS)[8] which incorporates a standard linear theory analysis[9,10] and a six-degree-of-freedom (6-DOF) nuemrical integration technique.[11]

The flight of each model was initially analyzed separately, then the flights at similar Mach numbers were simultaneously analyzed using the 6-DOF multiple fit technique. This provides a common set of aerodynamics that matched each of the separately measured position-attitude-time profiles. The multiple fit approach provides a more complete range of angle of attack and roll orientation combinations than would be available from any one flight considered separately. This increases the probability that the determined coefficients define the model's aerodynamics over the entire range of trajectories.

Table 1 Physical measurements and test conditions

Shot no.	Mach no.	$R_{e_L} \cdot 10^{-6}$	δ^2, deg	Model mass, gm	Xcg/L[a]
71	0.579	2.47	15.3	215.71	0.4820
72	0.586	2.52	3.9	216.47	0.4832
73	0.588	2.52	6.4	216.39	0.4845
74	0.722	3.11	9.9	214.11	0.4829
77	0.760	3.28	0.3	215.59	0.4811
75	0.773	3.31	0.6	220.76	0.4831
76	0.783	3.39	0.0	214.44	0.4826
81	1.028	4.44	28.4	216.64	0.4851
82	1.092	4.69	2.6	216.42	0.4814
87	1.243	5.40	72.6	216.16	0.4836
88	1.353	5.80	10.0	215.43	0.4835

[a]Measured from the nose.

Equations of Motion

The aerodynamic data presented in this paper were obtained using the fixed plane 6-DOF analysis (MLMFXPL).[11] The equations of motion are derived with respect to a fixed plane coordinate system. The x-axis points downrange, the y-axis points to the left looking downrange, and the z-axis points up. The 6-DOF differential equations of motion in this system are:

$$\dot{u} = g\sin\theta - qw + rv - a_{cu} + F_x/\bar{m} \tag{1}$$

$$\dot{v} = -ru - rw\tan\theta - a_{cv} + F_y/\bar{m} \tag{2}$$

$$\dot{w} = -g\cos\theta + rv\tan\theta + qu - a_{cw} + F_z/\bar{m} \tag{3}$$

and

$$\dot{p} = \ell/I_x \tag{4}$$

$$\dot{q} = -r^2\tan\theta - (I_x/I_y)rp + m/I_y \tag{5}$$

$$\dot{r} = qr\tan\theta + (I_x/I_y)qp + n/I_y \tag{6}$$

Once the definitions of the forces and moments are made, the solution of Eqs. (1-6) will define the 6-DOF flight motion of a symmetric missile in fixed plane coordinates. Since the position-attitude measurements, as required from a ballistic spark range, are obtained with respect to an Earth-fixed axis system, additional transformation equations are required. These transformation equations are shown below in terms of the fixed plane Euler angles (θ,ψ) and the angle of rotation about the missile axis (ϕ).

$$\dot{x} = u\cos\theta\cos\psi - v\sin\psi + w\sin\theta\cos\psi \tag{7}$$

$$\dot{y} = u\cos\theta\sin\psi + v\cos\psi + w\sin\theta\sin\psi \tag{8}$$

$$\dot{z} = -u\sin\theta + w\cos\theta \tag{9}$$

$$\dot{\theta} = q \tag{10}$$

$$\dot{\psi} = r/\cos\theta \tag{11}$$

$$\dot{\phi} = p + r\tan\theta \tag{12}$$

Coriolis accelerations (a_{cu}, a_{cv}, a_{cw}) are also included in Eqs. (1-3). The preceding Eqs. (1-12) are numerically integrated using a fourth-order Runge-Kutta scheme.

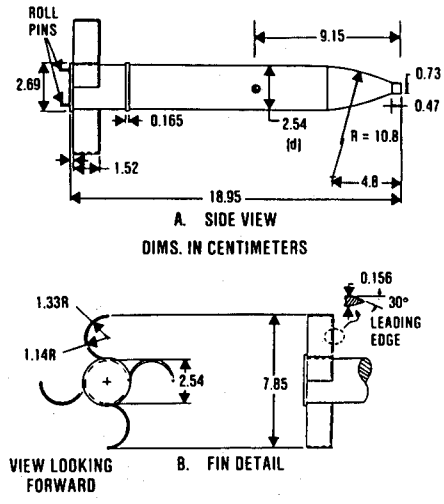

Fig. 1 Model configuration.

Aerodynamic Model

Initially, considerable difficulty was encountered in attempting to fit the experimentally measured trajectories associated with this WAF configuration. Various combinations of nonlinearities and roll dependencies were assumed; however, these fits failed to adequately match the experimentally measured motion patterns. It was suspected that the WAF were causing a side moment due to pitch (C_{n_α}). This out-of-plane moment was therefore added to the definition of the associated moment euqations and the fits reaccomplished. These fits successfully matched the solutions of the theoretical equations of motion to the experimentally measured motion patterns, indicating that this side moment due to pitch angle was present for this WAF configuration. The basic definitions of the aerodynamic forces and moments (including the C_{n_α} term), as used in obtaining the results reported herein, are shown below:

$$F_x = -\bar{q}AC_x \tag{13}$$

$$F_y = \bar{q}A\left[-\bar{C}_{N_\alpha}\frac{v}{V} + \frac{pd}{2V}\bar{C}_{Y_{p\alpha}}\frac{w}{V} + \bar{C}_{Y_{\gamma\alpha}}\frac{w}{V} + \bar{C}_{N_\delta}\delta_A\sin\phi - \bar{C}_{N_\delta}\delta_B\cos\phi\right] \tag{14}$$

$$F_z = \bar{q}A\left[-\bar{C}_{N_\alpha}\frac{w}{V} - \frac{pd}{2V}\bar{C}_{Y_{p\alpha}}\frac{v}{V} - \bar{C}_{Y_{\gamma\alpha}}\frac{v}{V} - \bar{C}_{N_\delta}\delta_A\cos\phi - \bar{C}_{N_\delta}\delta_B\sin\phi\right] \tag{15}$$

$$\ell = \bar{q}Ad\left[\frac{pd}{2V}\bar{C}_{\ell p} + \bar{C}_\ell\right] \tag{16}$$

$$m = \bar{q}Ad\left[\bar{C}_{m_\alpha}\frac{w}{V} + \frac{qd}{2V}\bar{C}_{mq} + \frac{pd}{2V}\bar{C}_{np_\alpha}\frac{v}{V} + \bar{C}_{n_{\gamma\alpha}}\frac{v}{V} + \bar{C}_{n_\alpha}\frac{v}{V} + \bar{C}_{m_\delta}\delta_A\cos\phi - \bar{C}_{m_\delta}\delta_B\sin\phi\right] \tag{17}$$

$$n = \bar{q}Ad\left[-\bar{C}_{m_\alpha}\frac{v}{V} + \frac{rd}{2V}\bar{C}_{mq} + \frac{pd}{2V}\bar{C}_{np_\alpha}\frac{w}{V} + \bar{C}_{n\gamma\alpha}\frac{w}{V} + \bar{C}_{n_\alpha}\frac{w}{V} + \bar{C}_{m_\delta}\delta_A\sin\phi + \bar{C}_{m_\delta}\delta_B\cos\phi\right] \tag{18}$$

The aerodynamic coefficients and derivatives, shown in Eqs. (13-18), were expanded as functions of Mach number, sine of the total angle of attack, and the aerodynamic roll angle. These expansions are shown in detail in Ref. 8. However, the side moment expansion was assumed to be linear, or $\bar{C}_n = C_n$ (thus $\bar{C}_{n_\alpha} = C_{n_\alpha}$).

Results

The aerodynamic coefficients and derivatives extracted from the experimentally measured trajectories are plotted in Figs. 2-6 and tabulated in Table 2. These figures show the zero angle-of-attack coefficients and derivatives obtained using the fixed plane 6-DOF analysis. The nonlinear terms obtained from the present analysis are shown in Table 2 and were derived using the multiple fit technique only. The multiple fit results would be expected to be superior to the analyses of the individual flights for the reasons previously discussed. However, some of the values obtained from the individual flights are plotted in Figs. 2-6 because they assist in showing the various trends in the data.

A cursory review of the data shown in Figs. 2-6 and Table 2 would not indicate any potential dynamic problems associated with this configuration. However, the models flown at supersonic velocities developed an increasing angle of attack history during their downrange trajectories, indicating a dynamic instability at the supersonic conditions. Typical angular motion plots for a subsonic, transonic, and supersonic flight are shown in Fig. 7 to illustrate this dynamic instability. Also notice the tendency of the motion patterns to become circular independent of whether the motion grows or damps.

Some of the models also displayed unusual roll characteristics; for example, the models tended to roll clockwise subsonically and counterclockwise supersonically. In the transonic region, roll reversals occurred on some flights. The roll profiles obtained from the various flights are shown in Fig. 8 along with the theoretical fits. Generally, the theoretical roll profiles matched the measured roll profiles reasonably well; nevertheless, the analysis routine had difficulty in determining the roll damping derivative ($C_{\ell p}$) as is evident from the values

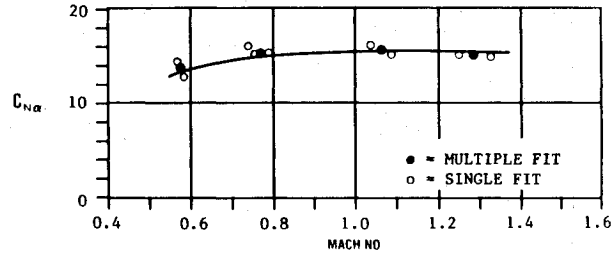

Fig. 2 Normal force derivative.

Table 2 6-DOF multiple fit results

Shot no.	Mach no.	C_{x0} $C_{x\alpha 2}$ $C_{x\alpha 4}$	$C_{N\alpha}$ $C_{N\alpha 3}$ $C_{N\alpha 5}$	$C_{m\alpha}$ $C_{m\alpha 3}$ $C_{m\alpha 5}$	C_{mq} C_{mq2} C_{mq4}	$C_{\ell\gamma\alpha 2}$ $C_{x\gamma\alpha 2}$ $C_{\ell p}$	C_{xM} $C_{m\alpha M}$ $C_{n\alpha}$
71,72,73	0.585	0.759	14.03	−46.249	−288.1	0.00	0.20
		2.000	0.00	785.040	0.0	0.00	0.00
		0.0	0.0	0.0	0.0	−22.385	−2.85
75,76,77	0.773	0.792	15.00	−52.045	−300.0	0.00	0.00
		2.000	9.00	0.000	0.0	0.00	0.00
		0.0	0.0	0.0	0.0	−3.473	−1.56
81,82	1.062	1.420	14.63	−41.192	−290.9	0.00	−0.40
		7.243	0.00	−223.010	0.0	0.00	62.11
		0.0	0.0	0.0	0.0	−27.990	−3.74
87,88	1.296	1.379	14.01	−32.549	−200.0	0.00	−0.20
		4.036	0.00	−143.530	0.0	0.00	0.00
		0.0	0.0	1163.7	0.0	−5.000	−3.57

listed in Table 2. These roll data have since been independently reanalyzed and the results presented in Ref. 12.

Although all the aerodynamic coefficients and derivatives presented in Figs. 3-6 and tabulated in Table 2 were obtained using the 6-DOF analysis techniques, linear theory fit parameters[9] such as vector magnitudes, vector frequencies, and damping rates are also shown in Table 3. When viewing these results, it should be remembered that the nutation vector can be either K_1 or K_2 depending on the direction of spin (p). By definition, the nutational vector rotates in the same direction as spin. For example, if the spin rate is negative, the nutation vector would be the one that has a negative frequency (ω_{20}).

Discussion

Initially it was suspected that the motion growth problem at supersonic Mach numbers, as shown in Fig. 7, was caused by a classic pitch-roll resonance. This is particularly true since the damping-in-pitch derivatives were negative (see Fig. 4) and the models displayed unusual roll characteristics, as described in the previous section. Also, the linear theory results, shown in Table 3, indicate that the supersonic flights, shots 87 and 88, were near resonance ($p/\omega_n \approx 1$). The motion growth caused by the resonant condition is due to an increase in the magnitude of the trim vector (K_T).[10,13] This increase in the magnitude of the trim vector is graphically portrayed in the sketch of Fig. 9 and shows that

$$/K_T/_{\text{res}} = (\text{amplification factor}) \cdot /K_T/_{p=0} \qquad (19)$$

Once the aerodynamic coefficients and derivatives have been determined for a particular configuration, the amplification factor (AF) can be approximated using the following relation[13]:

$$AF \approx \left(-\frac{md}{I_y \omega_N} Cm_\alpha\right) \Big/ \left[C_{N\alpha} - \frac{md^2}{I_y}(Cmq + Cm\dot{\alpha})\right] \qquad (20)$$

Thus, substituting in the measured physical properties of the models (Table 1) the determined aerodynamics (Figs. 2-6), the AF associated with the supersonic flights ($M \simeq 1.23$, shots 87 and 88) was computed to be about 12. Since these two flights were near resonance, it would therefore be expected that the trim vectors associated with these flights had increased to be no more than 12 times larger than the zero spin trim case. However, the 6-DOF analysis indicated that the zero spin trim vectors were small, less than 0.25 deg. In fact, the trim vectors were so small that linear theory could not determine the magnitude of K_T, and they were assumed to be zero. Therefore, the motion growth related to the resonance condition would be expected to be less than 3 deg. This obviously does not account for the motion growth, shown in Fig. 7, for

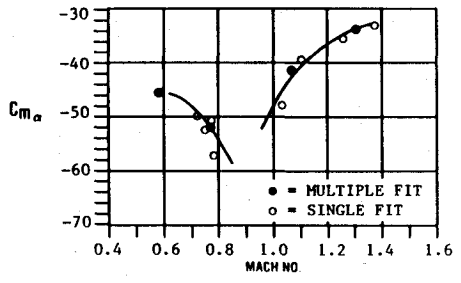

Fig. 3 Pitching moment derivative.

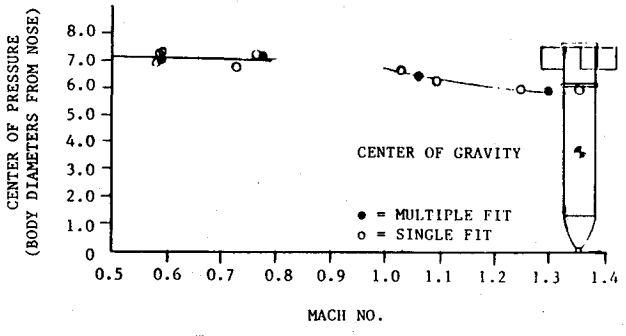

Fig. 5 Location of the center of pressure.

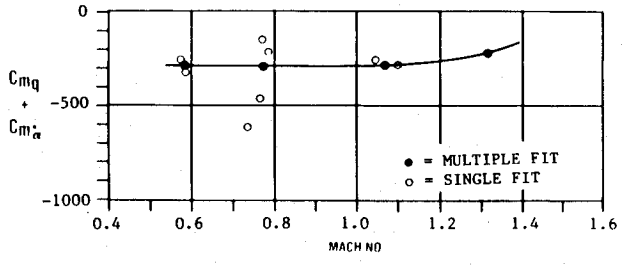

Fig. 4 Damping-in-pitch derivatives.

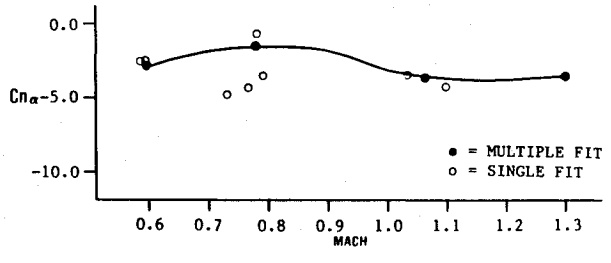

Fig. 6 Side moment derivative.

Table 3 Linear theory fit parameters

Shot no.	Mach no.	$\bar{\delta}^2$ deg^2	$K10$, deg	$K20$, deg	λ_1, $1/M$	λ_2, $1/M$	P/ω_N
71	0.579	15.3	3.34	4.21	−0.04871	−0.00560	0.29
72	0.586	3.9	3.40	1.64	−0.04858	−0.00842	0.30
73	0.588	6.4	2.57	2.74	−0.05107	−0.00730	0.03
74	0.722	9.9	1.34	4.47	−0.04094	−0.01196	0.04
77	0.760	0.3	0.63	0.67	−0.02850	−0.00695	0.22
75	0.773	0.6	0.67	1.46	−0.03640	−0.02280	0.03
76	0.783	0.0	0.17	0.18	−0.02625	−0.02297	0.45
81	1.028	28.4	2.94	5.17	−0.04990	0.00007	0.05
82	1.092	2.6	0.21	1.18	−0.02998	0.00650	0.41
87	1.243	72.6	0.80	4.82	−0.01410	0.00976	1.07
88	1.353	10.0	0.30	3.20	−0.01312	−0.00067	0.91

the supersonic flight of shot 87, and the cause of this dynamic instability must be found elsewhere.

The only other unconventional aspect of the 6-DOF analysis was the addition of the side moment derivative due to pitch. As was previously discussed, this derivative ($C_{n\alpha}$) was included in the moment equations in order to adequately fit the measured motion patterns. The question then becomes: Can this side moment be causing the dynamic instability problems at the supersonic conditions? The tendency of the motion to develop into a circular pattern (as mentioned in the previous section) provides a clue to the possible effects of this side moment. Both Murphy[10] and Nicolaides[13] have studied the consequences of a side moment due to pitch on the dynamic stability of a finned missile. The equations for the computation of the nutational and precessional damping rates, as expressed by Nicolaides,[13] including $C_{n\alpha}$, are shown as follows:

$$\lambda_1 = \frac{\rho A}{4\bar{m}}\left[-C_{N\alpha}\left(1-\frac{1}{\sigma}\right)+(C_{mq}+C_{m\dot{\alpha}})\left(\frac{\bar{m}d^2}{2I_y}\right)\left(1+\frac{1}{\sigma}\right)+\frac{\bar{m}d^2}{I_x}\left(\frac{1}{\sigma}\right)C_{n\alpha}\left(\frac{2V}{pd}\right)\right] \tag{21}$$

$$\lambda_2 = \frac{\rho A}{4\bar{m}}\left[-C_{N\alpha}\left(1+\frac{1}{\sigma}\right)+(C_{mq}+C_{m\dot{\alpha}})\left(\frac{\bar{m}d^2}{2I_y}\right)\left(1-\frac{1}{\sigma}\right)-\frac{\bar{m}d^2}{I_x}\left(\frac{1}{\sigma}\right)C_{n\alpha}\left(\frac{2V}{pd}\right)\right] \tag{22}$$

where

$$\sigma = \sqrt{1-\frac{1}{S_g}} \tag{23}$$

and

$$S_g = \frac{2I_x^2 p^2}{\pi\rho I_y C_{m\alpha} d^3 V^2} \tag{24}$$

Equations (21) and (22) assume that the Magnus moment is negligible and, substituting in the measured physical properties and the determined aerodynamic derivatives at the test Mach numbers, the associated damping rates were computed. These computations are listed in Table 4 for various values of $C_{n\alpha}$ and spin. As is shown for Mach 0.57, the damping rates, (λ_1 and λ_2), were insensitive to variations in the spin rate (p), from near zero to resonance. However, variations in the side moment derivative, ($C_{n\alpha}$), from -1 to -5 significantly altered the computed damping rates. Since the damping rates were shown to be insensitive to spin at Mach 0.59, the computations for Mach numbers of 0.77, 1.06, and 1.30 used a spin rate of about one-half resonance. The computed λ_2 values show that as $C_{n\alpha}$ is varied from -1 to -5, this damping rate tends to become positive (undamped). Also this undamping trend appears to get more severe as the Mach number increases. In fact, at Mach 1.3 a $C_{n\alpha}$ value of -3 causes an undamped λ_2. It should be noted that this value of -3 for $C_{n\alpha}$ at Mach 1.3 is about what $C_{n\alpha}$ was determined to be from the 6-DOF analysis (see Fig. 6). Also the trends in the computed λ_2 values shown in Table 4 agree well with the measured linear theory values listed in Table 3. It was therefore concluded that

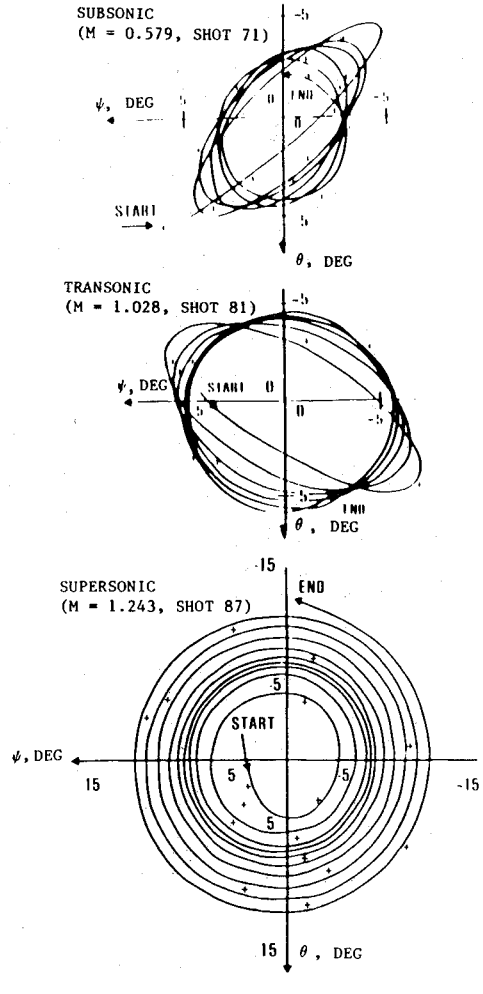

Fig. 7 Typical angular motion plots.

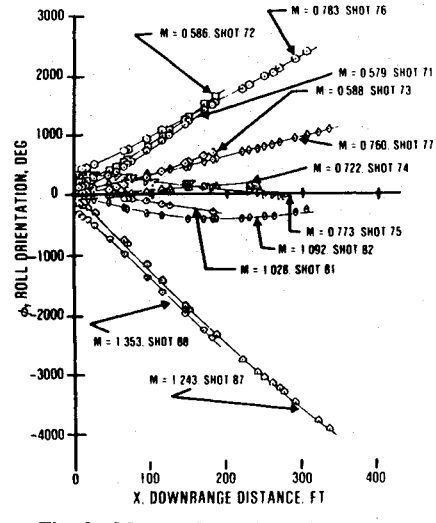

Fig. 8 Measured and fitted roll profiles.

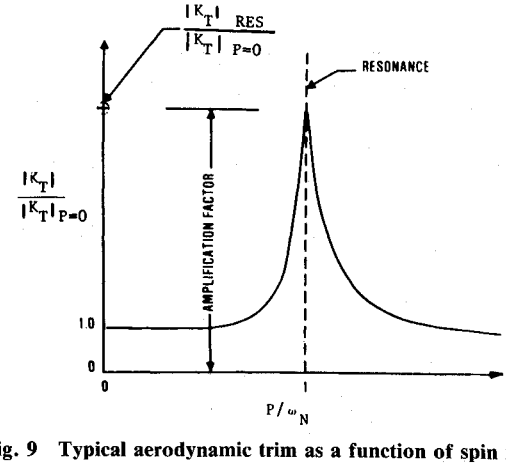

Fig. 9 Typical aerodynamic trim as a function of spin rate.

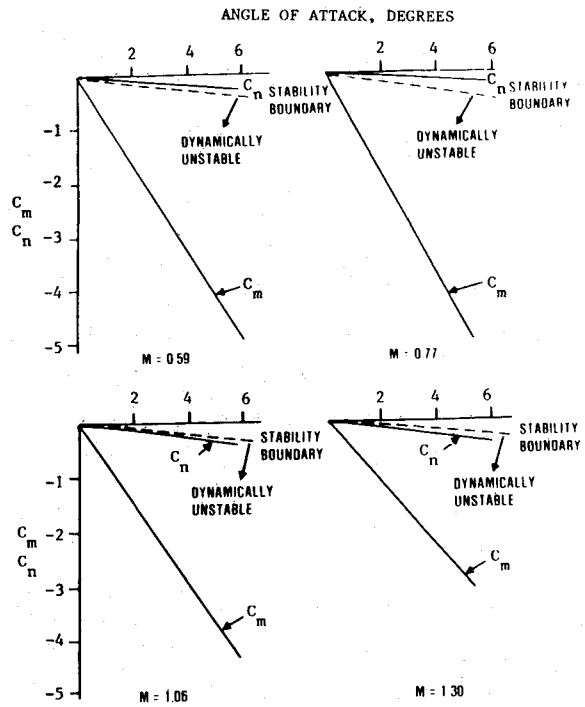

Fig. 10 Dynamic stability boundary conditions.

Table 4 Dynamic stability computations

Mach	$C_{n\alpha}$	P, rad/s	λ_1, $1/M$	λ_2, $1/M$
0.59	−1.0	0.1	−0.0366	−0.0216
0.59	−1.0	70.2	−0.0367	−0.0215
0.59	−1.0	140.4	−0.0367	−0.0214
0.59	−3.0	0.1	−0.0516	−0.0065
0.59	−3.0	70.2	−0.0517	−0.0065
0.59	−3.0	140.4	−0.0518	−0.0064
0.59	−5.0	0.1	−0.0666	+0.0085
0.59	−5.0	70.2	−0.0667	+0.0086
0.59	−5.0	140.4	−0.0668	+0.0086
0.77	−1.0	93.5	−0.0377	−0.0234
0.77	−3.0	93.5	−0.0519	−0.0093
0.77	−5.0	93.5	−0.0660	+0.0048
1.06	−1.0	128.7	−0.0377	−0.0216
1.06	−3.0	128.7	−0.0536	−0.0057
1.06	−5.0	128.7	−0.0695	+0.0102
1.30	−1.0	152.0	−0.0323	−0.0142
1.30	−3.0	152.0	−0.0503	+0.0038
1.30	−5.0	152.0	−0.0683	+0.0218

this side moment, which appears to be symptomatic of WAF configurations, is the cause of the dynamic instability as measured at the supersonic condition.

The stability boundaries can also be determined by setting λ_2 equal to zero in Eq. (22) and solving for $C_{n\alpha}$. These stability boundaries are shown in Fig. 10 along with the determined slopes of C_m and C_n for each of the test Mach numbers. This figure confirms that subsonically the determined side moments fall in the dynamically stable region; whereas, supersonically, the side moments are dynamically destabilizing. This figure also indicates that the stable region is decreasing with Mach number; or, that very small values of $C_{n\alpha}$ can cause a dynamic instability at Mach 1.3.

Conclusions

The results of a free-flight range test of a WAF configuration at subsonic and transonic Mach numbers indicated that an out-of-plane side moment due to pitch angle was prevalent. This side moment caused a dynamic instability at the supersonic Mach numbers. Linear theory accurately predicts this dynamic instability assuming that the side moment has been measured. It is suspected that this side moment is symptomatic of WAF configurations; when testing such configurations, the test engineer should ensure that this side moment is obtained and the stability boundaries are computed. Designers of such configurations should also consider the possibility of this side moment because it can have a dramatic effect on trajectory computations based on the conventional aerodynamic coefficients and derivatives.

References

[1]Dahlke, C. W. and Flowers, L. D., "The Aerodynamic Characteristics of Wraparound Fins, Including Fold Angle at Mach Numbers from 0.5 to 1.3," U.S. Army Missile Research and Development Command, Redstone Arsenal, AL, TR-RD-75-19, Dec. 1974.

[2]Humphrey, James A. and Dahlke, C. W., "A Summary of Aerodynamic Characteristics for Wraparound Fins from Mach 0.3 to 3.0," U.S. Army Missile Research and Development Command, Redstone Arsenal, AL, TR-TD-77-5, Mar. 1977.

[3]Pope, R. L. and Dudley, R. E., "Flight Tests of the MK IV Wraparound Fin Configuration," Weapons Systems Research Laboratory, Defense Research Center, Salisbury, South Australia, WSRL-0252 TR, Jan. 1982.

[4]Dahlke, C. W. and Craft, J. C., "The Effect of Wraparound Fins on Aerodynamic Stability and Rolling Moment Variations," U.S. Army Missile Research and Development Command, Redstone Arsenal, AL, TR-RD-17, July 1973.

[5]Hardy, Samuel R., "Nonlinear Analysis of the Rolling Motion of a Wraparound Fin Missile at Angles of Attack from 0 to 90 Degrees in Incompressible Flow," Naval Surface Weapons Center, Dahlgren, VA, NSWCDL-TR-3727, Sept. 1977.

[6]Cohen, C. J., Clare, T. A., and Steens, F. L., "Analysis of the Nonlinear Rolling Motion of Finned Missile," AIAA Paper 72-980, 1972.

[7]Winchenbach, G., Galanos, D., Kleist, J., and Lucas, B., "Description and Capabilities of the Aeroballistic Research Facility," USAF Armament Laboratory, Eglin AFB, FL, AFATL-TR-78-41, Feb. 1978.

[8]Whyte, R. H., Winchenbach, G., and Hathaway, W. H., "Subsonic Free Flight Data for a Complex Asymmetric Missile," *Journal of Guidance, Control, and Dynamics*, Vol. 4, Jan.-Feb. 1981, pp. 59-65.

[9]Murphy, C. H., "Data Reduction for the Free Flight Spark Ranges," U.S. Army Ballistic Research Laboratory, Aberdeen, MD, BRL-Report 900, Feb. 1954.

[10]Murphy, C. H., "Free Flight Motion of Symmetric Missile," U.S. Army Ballistic Research Laboratory, Aberdeen, MD, BRL-Report 1216, July 1963.

[11]Winchenbach, G. L., Uselton, R. L., Hathaway, W. H., and Chelekis, R. M., "Free Flight and Wind Tunnel Data for a Generic Fighter Configuration," *Journal of Aircraft*, Vol. 21, Jan. 1984, pp. 5-13.

[12]Kim, Young Hoon, Winchenbach, G. L., "The Roll Motion of a Wraparound Fin Configuration at Subsonic and Transonic Mach Numbers," AIAA Paper 85-1777, Aug. 1985.

[13]Nicolaides, J. D., "Free Flight Dynamics," University of Notre Dame, South Bend, IN, 1968.